APPLICATION OF TURBULENCE MODELS IN THE NAVIER-STOKES EQUATIONS RESOLUTION FOR A HYDRAULIC JUMP TRANSIENT PROBLEM

APLICAÇÃO DE MODELOS DE TURBULÊNCIA NA RESOLUÇÃO DAS EQUAÇÕES DE NAVIER-STOKES PARA UM PROBLEMA TRANSIENTE DE RESSALTO HIDRÁULICO

Alexandre Botari[1]
Eudes José Arantes[2]

Abstract. This paper proposes to present an application of CFD programs in a simulation of the flow in a hydraulic jump. Initially, it has been introduced the nonlinear representative equations of the flow and the turbulence models necessary to solve Navier-Stokes equations. Therefore, it will be demonstrated how to resolve these equations using the numerical methods by means of discretisetion and system solve. Finally, it will be shown a transient problem application in a simulation of a hydraulic jump of horizontal channel. The turbulence model used for proposed problem resolution was the Reynolds Stress Model (RSM), which better represents the physical flow characteristics of the problem. A comparison of the numerical results with experimental data has showed two different behaviors: the free surface in the experimental data presents the level of upstream agreement higher than in the hydraulic jump, therefore, in the first one the experimental data line was immerged in to 90% of volume fraction of water region, by the other hand, in the hydraulic jump, the experimental free surface is in between 70 and 80% of volume fraction of water region.

Keywords: Mathematical model; CFD tool; Mass Balance; Control volume.

Resumo: Este trabalho propõe a aplicação de modelos matemáticos via programa CFD em uma simulação de escoamento em um ressalto hidráulico. Inicialmente, foram introduzidas as equações não-lineares e representativas do escoamento e dos modelos de turbulência necessários para resolver equações de Navier-Stokes. Serão apresentadas as formas de resolução destas equações usando-se os métodos numéricos por meio da discretização das equações do sistema. Finalmente, será aplicado na solução de um problema transiente na simulação de um ressalto hidráulico em canal horizontal. O modelo de turbulência usado para resolução do problema proposto foi o modelo de Stress de Reynolds (RSM), que melhor representa as características físicas e de escoamento do problema proposto. Uma comparação dos resultados numéricos com dados experimentais mostrou dois comportamentos diferentes: na superfície livre à montante do ressalto hidráulico a simulação apresenta um nível de aproximação mais elevado do que no salto hidráulico propriamente dito, da ordem de cerca de 90% comparando-se com os dados experimentais, por outro lado, no ressalto hidráulico a imersão da superfície livre situou-se entre 70 e 80% do total dos resultados simulados comparando-se com os dados experimentais para esta região.

Palavras-chave: Modelo matemático; ferramenta CFD; Balanço de massa; Volume de controle.

[1] Professor Adjunto do Departamento de Tecnologia DTC do Centro de Tecnologia CTC da Universidade Estadual de Maringá – UEM.
[2] Professor da Universidade Tecnológica Federal do Paraná – UTFPR de Campo Mourão.

1 INTRODUCTION

Computational Fluid Dynamics (CFD) is a computer-based tool for simulating the behavior of systems involving fluid flow, heat transfer, and other related physical processes. It works by solving the equations of fluid flow (in a special form) over a region of interest, with specified (known) conditions on the boundary of that region.

Computers have been used to solve fluid flow problems for many years. Numerous programs have been written to solve either specific problems, or specific classes of problem. From the mid-1970's the complex mathematics required to generalize the algorithms began to be understood, and general-purpose CFD solvers were developed. These began to appear in the early 1980's and required what were then very powerful computers, as well as an in-depth knowledge of fluid dynamics, and large amounts of time to set up simulations. Consequently, CFD was a tool used almost exclusively in research. Recent advances in computing power, together with powerful graphics and interactive 3-D manipulation of models mean that the process of creating a CFD model and analyzing the results is much less labor-intensive, reducing the time and therefore the cost. Advanced solvers contain algorithms, which enable robust solution of the flow field in a reasonable time. As a result of these factors, Computational Fluid Dynamics is now an established industrial design tool, helping to reduce design timescales and improve processes throughout the engineering world. CFD provides a cost-effective and accurate alternative to scale model testing, with variations on the simulation being performed quickly; offering obvious advantages (CFX, 2004).

The set of equations that describe the processes of momentum, heat and mass transfer are known as the Navier-Stokes equations. These partial differential equations were derived in the early nineteenth century. They have no known general analytical solution but can be discretised and solved numerically. Equations describing other processes, such as combustion, can also be solved in conjunction with the Navier-Stokes equations. Often, an approximating model is used to derive these additional equations, turbulence models being a particularly important example. There are a number of different solution methods that are used in CFD codes. The most common, and the one on which Software is based, is known as the finite volume technique. In this technique, the region of interest is divided into small sub-regions, called control volumes. The equations are discretised and solved iteratively for each control volume. As a result, an approximation of the value of each variable at specific points throughout the domain can be obtained. In this way, one derives a full picture of the behavior of the flow (CFX, 2004).

This paper proposes to present an application of CFD programs in a simulation of the flow in a hydraulic jump. Initially, it has been introduced the nonlinear representative equations of the flow and the turbulence models necessary to solve Navier-Stokes equations. Therefore, it will be demonstrated how to resolve theses equations using the numerical methods by means of discretisetion and system solve. Finally, it will be shown a transient problem application in a simulation of a hydraulic jump of horizontal channel. The turbulence model used for proposed problem resolution was the Reynolds Stress Model (RSM), which better represents the physical flow characteristics of the problem.

2 TRANSPORT EQUATIONS

The hypothesis being considered of the continuous and the Newtonian fluids (Figure 1), the equations associated to the conservation beginnings are had (LESIEUR, 1996).

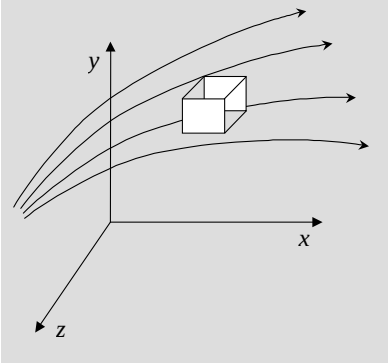

Figure 1. Control Volume for Mass Balance and Momentum

- The Continuity Equation.

$$\underbrace{\frac{\partial \rho}{\partial t}}_{\substack{\text{Mass Variation Rate} \\ \text{in the Control Volume}}} + \underbrace{\nabla.(\rho \boldsymbol{u})}_{\substack{\text{Mass Flow through} \\ \text{the Surface of the Control Volume}}} = 0 \qquad (1)$$

where: $\boldsymbol{u}$ is the velocity vector and ρ is the fluid density.

- The Momentum Equations (The Navier-Stokes Equations). $m\boldsymbol{a} = F_{surface} + F_{body}$

where: *F* is force e *m* is mass and: $\boldsymbol{a} = \frac{D\boldsymbol{u}}{Dt} = \frac{\partial(\boldsymbol{u})}{\partial t} + (\boldsymbol{u}.\nabla)(\boldsymbol{u})$ = is acceleration.

Using the compressible flow and constant physical properties hypothesis, it is had:

$$\underbrace{\frac{\partial \rho u}{\partial t}}_{\substack{\text{Momentum} \\ \text{Variation Rate}}} + \underbrace{(u.\nabla)\rho u}_{\substack{\text{Convective Flow} \\ \text{of the Momentum}}} = \underbrace{-\nabla p}_{\text{Press Gradient Force}} + \underbrace{\mu \nabla^2 u}_{\substack{\text{Diffusive Flow of the Momentum} \\ \text{or Dissipation Kinetic Energy}}} \qquad (2)$$

where: $\boldsymbol{p}$ is the pressure, μ is cinematic dynamic and *t* is the time.

The convective flow term of the momentum also expresses the non-lineal interactions among the several scales that compose the spectrum of energy typical of the flow.

- The Energy Equation.

$$\underbrace{\frac{\partial T}{\partial t}}_{\substack{\text{Energy} \\ \text{Variation Rate}}} + \underbrace{(\boldsymbol{u}.\nabla)T}_{\substack{\text{Energy} \\ \text{Convective Flow}}} = \underbrace{\alpha \nabla^2 T}_{\substack{\text{Energy} \\ \text{Diffusive Flow}}} + \underbrace{S_E}_{\text{Energy Source}} \qquad (3)$$

where: *T* is the temperature; α is thermal conductivity; S_E is the energy source.

3 REYNOLDS AVERAGE NAVIER-STOKES (RANS)

The basics Navier-Stokes equations are modified to represent the instantaneous variable how an average variable composition. Using the average functions proprieties, the equation for the average flow is obtained. These news equations, due to the original non-linear equations, contain terms that involve the products of speeds buoyancy in different directions. Theses buoyancy terms do not have the definitive equation and give origin the eddy viscosity. For example, a velocity vector $\boldsymbol{u}$ may be divided into an average component, $\overline{\boldsymbol{u}}$, and a time varying component, $\boldsymbol{u}'$ (LESIEUR, 1996).

$$\boldsymbol{u} = \bar{\boldsymbol{u}} + \boldsymbol{u}'$$

The averaged component is given by: $\bar{\boldsymbol{u}} = \frac{1}{\Delta t}\int_{t}^{t+\Delta t} \boldsymbol{u}.dt$

The Equations below shows the Reynolds Equation for the incompressible flow.

$$\frac{\partial \rho}{\partial t} + \nabla \cdot (\rho \bar{\boldsymbol{u}}) = 0 \quad (4)$$

$$\frac{\partial \rho \bar{\boldsymbol{u}}}{\partial t} + \nabla .\ (\rho\ \bar{\boldsymbol{u}} \times \bar{\boldsymbol{u}}) \ = \ \nabla .\ (\tau - \rho \overline{\boldsymbol{u}' \times \boldsymbol{u}'}) \ + S_M \quad (5)$$

where: $\tau = \mu.\nabla.\bar{\boldsymbol{u}}$ is the molecular stress tensor, S_M is source term of momentum equation.

$$\frac{\partial \rho \phi}{\partial t} + \nabla .\ (\rho\ \bar{\boldsymbol{u}} \phi) \ = \ \nabla .\ (\Gamma \nabla \phi - \rho \overline{\boldsymbol{u}' \phi}) \ + S_\phi \quad (6)$$

where: $\emptyset$ is transport variable; Γ is diffusivity and $S_\emptyset$ is source term of transport equation.

The continuity equation has not been altered but the momentum and scalar transport equations contain turbulent flux terms additional to the molecular diffusive fluxes. These are the Reynolds stress, $\rho \overline{\boldsymbol{u}' \times \boldsymbol{u}'}$, and the Reynolds flux, $\rho \overline{\boldsymbol{u}' \phi}$. These terms arise from the nonlinear convective term in the un-averaged equations. They reflect the fact that convective transport due to turbulent velocity fluctuations will act to enhance mixing over and above that caused by thermal fluctuations at the molecular level. At high Reynolds numbers, turbulent velocity fluctuations occur over a length scale much larger than the mean free path of thermal fluctuations, so that the turbulent fluxes are much larger than the molecular fluxes (CFX, 2004).

4 TURBULENCE MODELS

Turbulent flows are characterized by fluctuating velocity fields. These fluctuations mix transported quantities such as momentum, energy, and species concentration, and cause the transported quantities to fluctuate as well. Since these fluctuations can be of small scale and high frequency, they are too computationally expensive to simulate directly in practical engineering calculations. Instead, the instantaneous (exact) governing equations can be time-averaged, ensemble-averaged, or otherwise manipulated to remove the small scales, resulting in a modified set of equations that are computationally less expensive to solve. However, the modified equations contain additional unknown variables, and turbulence models are needed to determine these variables in terms of known quantities (WILCOX, 2000).

The highlights turbulences models in the bibliographies are presented below.

- One Equation Model.
  - Spalart-Allmaras model.
- Two Equations Models.]
- $k - \varepsilon$ Model
  - Standard $k - \varepsilon$ Model.
  - Renormalization-group (RNG) $k - \varepsilon$ Model.
  - Realizable $k - \varepsilon$ Model.
- $k - \omega$ Model.
  - Standard $k - \omega$ Model.
  - Shear stress transport (SST) $k - \omega$ Model.
- $v^2 - f$ Model.

- Reynolds stress model (RSM)
- Large eddy simulation (LES) model
- Detached Eddy Simulation (DES) model.

In the above item, have being increase computational effort in the models upper to down, due to physics variable additions (WILCOX, 2000).

In this problem, the Turbulence Model used for calculation was The Reynolds Stress Model.

4.1 THE REYNOLDS STRESS MODEL (RSM)

The Reynolds Stress Model involves calculation of the individual Reynolds Stresses, $\overline{\boldsymbol{u}'\times\boldsymbol{u}'}$, using differential transport equations. The individual Reynolds stresses are then used to obtain closure of the Reynolds-averaged momentum equation.

The exact form of the Reynolds stress transport equations may be derived by taking moments of the exact momentum equation. This is a process wherein the exact momentum equations are multiplied by a fluctuating property, the product then being Reynolds-averaged. Unfortunately, several of the terms in the exact equation are unknown and modeling assumptions are required in order to close the equations. The Reynolds stress transport equations are presented together with the modeling assumptions required to attain closure.

The exact transport equations for the transport of the Reynolds stresses, $\rho\,\overline{\boldsymbol{u}'\times\boldsymbol{u}'}$, may be written as follows (LAUNDER ET AL., 1975) (SMAGORINSKY, 1963):

$$\frac{\partial\rho\,\overline{\boldsymbol{u}'\times\boldsymbol{u}'}}{\partial t}+\nabla\cdot\left(\rho\,\overline{\boldsymbol{u}'\times\boldsymbol{u}'}\times\boldsymbol{u}\right)-\nabla\cdot\left(\rho C\frac{k}{\varepsilon}\overline{\boldsymbol{u}'\times\boldsymbol{u}'}\left(\nabla\overline{\boldsymbol{u}'\times\boldsymbol{u}'}\right)^{T}\right)=\boldsymbol{P}+\boldsymbol{G}+\varphi-\frac{2}{3}\delta\rho\varepsilon \tag{7}$$

where $\boldsymbol{P}$ and $\boldsymbol{G}$ are shear and buoyancy turbulence production terms of the Reynolds stresses respectively and C is a constant. Buoyancy turbulence terms are controlled in the same way as for the k-□ and k-□ model.

The transport of the Reynolds stresses can be written in index notation as.

$$\frac{\partial}{\partial t}\left(\rho\overline{u'_i\,u'_j}\right)+\frac{\partial}{\partial x_k}\left(u_k\rho\,\overline{u'_i\,u'_j}\right)=P_{ij}+\phi_{ij}+\frac{\partial}{\partial x_k}\left[\left(\mu+\frac{2}{3}c_S\rho\frac{k^2}{\varepsilon}\right)\frac{\partial\overline{u'_i\,u'_j}}{\partial x_x}\right]-\frac{2}{3}\delta_{ij}\rho\varepsilon \tag{8}$$

where □$_{ij}$ is the pressure-strain correlation, and P_{ij}, the exact production term, is given by:

$$P_{ij}=-\rho\left(\overline{u'_i u'_k}\frac{\partial u_j}{\partial x_k}+\overline{u'_j u'_k}\frac{\partial u_i}{\partial x_k}\right) \tag{9}$$

As the turbulence dissipation appears in the individual stress equations, an equation for e is still required. This now has the form:

$$\frac{\partial(\rho\varepsilon)}{\partial t}+\frac{\partial}{\partial x_k}(\rho u_k\varepsilon)=\frac{\varepsilon}{k}(c_{\varepsilon 1}P-c_{\varepsilon 2}\rho\varepsilon)+\frac{\partial}{\partial x_k}\left[\left(\mu+\frac{\mu_t}{\sigma_\varepsilon}\right)\frac{\partial\varepsilon}{\partial x_k}\right] \tag{10}$$

One of the most important terms in Reynolds stress models is the pressure-strain correlation, □$_{ij}$.

The pressure strain correlations can be expressed in the general form:

$$\phi_{ij}=\phi_{ij,1}+\phi_{ij,2}+\phi_{ij,w} \tag{11}$$

where $\phi_{ij,1}$ is the slow pressure-strain term, also known as the return-to-isotropy term, $\phi_{ij,2}$ is called the rapid pressure-strain term, and $\phi_{ij,w}$ is the wall-reflection term.

The slow pressure-strain term, $\phi_{ij,1}$, is modeled as.

$$\phi_{ij,1} = C_1 \rho \frac{\varepsilon}{k}\left(\overline{u_i' u_j'} - \frac{2}{3}\delta_{ij} k\right) \tag{12}$$

with $C_1 = 1{,}8$.

The rapid pressure-strain term, $\phi_{ij,2}$, is modeled as.

$$\phi_{ij,2} = -C_2\left[\left(P_{ij} - C_{ij}\right) - \frac{2}{3}\delta_{ij}\left(P + C\right)\right] \tag{13}$$

where $C_2 = 0{,}60$, P_{ij} is defined as in Equation 9, and C_{ij} is convection term in the transport of the Reynolds stress equation, $P = \frac{1}{2}P_{kk}$ and $C = \frac{1}{2}C_{kk}$.

The wall-reflection term, $\phi_{ij,w}$, is responsible for the redistribution of normal stresses near the wall. It tends to damp the normal stress perpendicular to the wall, while enhancing the stresses parallel to the wall. This term is modeled as equations (4) and (5).

$$\phi_{ij,w} = C_1' \frac{\varepsilon}{k}\left(\overline{u_k' u_m'} n_k n_m \delta_{ij} - \frac{3}{2}\overline{u_i' u_k'} n_j n_k - \frac{3}{2}\overline{u_j' u_k'} n_i n_k\right)\frac{k^{3/2}}{C_\ell \, \varepsilon \, d}$$

$$+ C_2'\left(\phi_{km,2} n_k n_m \delta_{ij} - \frac{3}{2}\phi_{ik,2} n_j n_k - \frac{3}{2}\phi_{jk,2} n_i n_k\right)\frac{k^{3/2}}{C_\ell \, \varepsilon \, d} \tag{14}$$

where $C_1' = 0{,}5$; $C_2' = 0{,}3$; n_k is the x_k component of the unit normal to the wall, d is the normal distance to the wall, and $C_\ell = C_\mu^{3/4}/\kappa$, where $C_\mu = 0{,}09$ and κ is the von Kármán constant ($\kappa = 0{,}4187$).

5 NUMERICAL DISCRETISATION

Analytical solutions to the Navier-Stokes equations exist for only the simplest of flows under ideal conditions. To obtain solutions for real flows a numerical approach must be adopted whereby the equations are replaced by algebraic approximations, which may be solved using a numerical method.

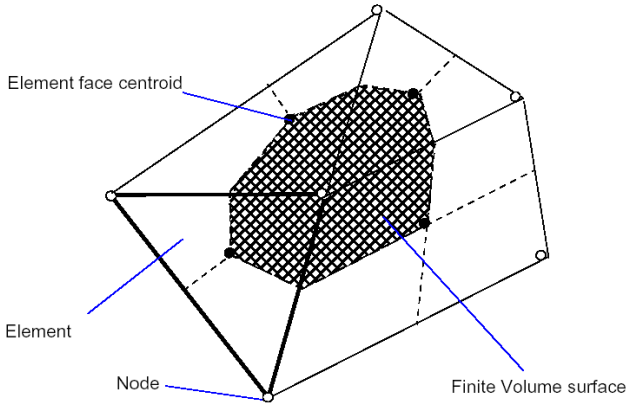

Figure 2. Volume Finite Surface (CFX, 2004)

This approach involves discretising the spatial domain into finite control volumes using a mesh. The governing equations are integrated over each control volume, such that the relevant quantity (mass, momentum, energy etc.) is conserved in a discrete sense for each control volume. The Figure 2 shows a typical mesh with unit depth (so that it is two-dimensional), on which one surface of the finite volume is represented by the shaded area [1].

It is clear that each node is surrounded by a set of surfaces, which comprise the finite volume. All the solution variables and fluid properties are stored at the element nodes. Consider the mean form of the conservation equations for mass, momentum and a passive scalar, expressed in Cartesian coordinates (CFX, 2004):

$$\frac{\partial \rho}{\partial t} + \frac{\partial (\rho u_j)}{\partial x_j} = 0 \tag{15}$$

$$\frac{\partial}{\partial t}(\rho u_i) + \frac{\partial}{\partial x_j}(\rho u_j u_i) = -\frac{\partial P}{\partial x_i} + \frac{\partial}{\partial x_j}\left(\mu_{eff}\left(\frac{\partial u_i}{\partial x_j} + \frac{\partial u_j}{\partial x_i}\right)\right) \tag{16}$$

$$\frac{\partial}{\partial t}(\rho \phi) + \frac{\partial}{\partial x_j}(\rho u_j \phi) = \frac{\partial}{\partial x_j}\left(\Gamma_{eff}\left(\frac{\partial \phi}{\partial x_j}\right)\right) + S_\phi \tag{17}$$

where: $\Gamma_{eff} = \Gamma + \Gamma_T$; Γ_T is the turbulence diffusivity.

These equations are integrated over a control volume, and Gauss' divergence theorem is applied to convert some volume integrals to surface integrals. For control volumes that do not deform in time, the time derivatives can be moved outside of the volume integrals and the equations become:

$$\frac{d}{dt}\int_V \rho dV + \int_S \rho u_j dn_j = 0 \tag{18}$$

$$\frac{d}{dt}\int_V \rho u_i dV + \int_S \rho u_j u_i dn_j = -\int_S P dn_j + \int_S \mu_{eff}\left(\frac{\partial u_i}{\partial x_j} + \frac{\partial u_j}{\partial x_i}\right) dn_j + \int_V S_{u_i} dV \tag{19}$$

$$\frac{d}{dt}\int_V \rho \phi dV + \int_S \rho u_j \phi dn_j = \int_S \Gamma_{eff}\left(\frac{\partial \phi}{\partial x_j}\right) dn_j + \int_V S_\phi dV \tag{20}$$

where V and s respectively denote volume and surface regions of integration, and dn_j are the differential Cartesian components of the outward normal surface vector. The surface integrals are the integrations of the fluxes, whereas the volume integrals represent source or accumulation terms. Changes to these equations due to control volume deformation are presented below.

The first step in solving these continuous equations numerically is to approximate those using discrete functions. Now consider an isolated mesh element such as the one shown below.

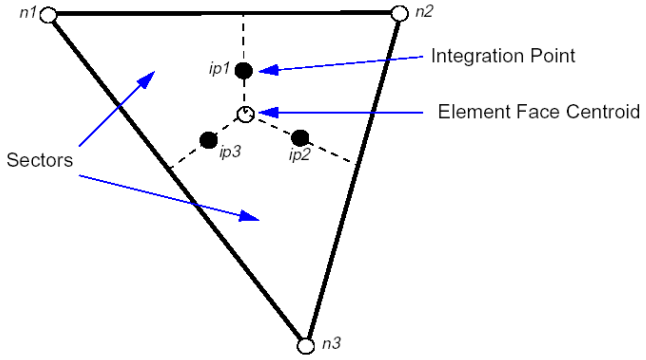

Figure 3. Isolated Mesh Element (CFX, 2004).

The surface fluxes must be discretely represented at the integration points to complete the conversion of the continuous equation into their discrete form. The integration points, *ipn*, are located at the centre of each surface segment in a 3D element surrounding the finite volume.

The discrete form of the integral equations is written as (CFX, 2004):

$$\rho V\left(\frac{\rho-\rho^{o}}{\Delta t}\right)+\sum_{ip}\left(\rho u_{j}\Delta n_{j}\right)_{ip}=0 \qquad V\left(\frac{\rho-\rho^{o}}{\Delta t}\right)+\sum_{ip}\left(\rho u_{j}\Delta n_{j}\right)_{ip}=0 \tag{21}$$

$$\rho V\left(\frac{u_{i}-u_{i}^{o}}{\Delta t}\right)+\sum_{ip}\dot{m}_{ip}\left(u_{i}\right)_{ip}=\sum_{ip}\left(P\Delta n_{i}\right)_{ip}+\sum_{ip}\left(\mu_{eff}\left(\frac{\partial u_{i}}{\partial x_{j}}+\frac{\partial u_{j}}{\partial x_{i}}\right)\Delta n_{j}\right)_{ip}+\overline{S_{M_{i}}}V \tag{22}$$

$$\rho V\left(\frac{\phi-\phi^{o}}{\Delta t}\right)+\sum_{ip}\dot{m}_{ip}\phi_{ip}=\sum_{ip}\left(\Gamma_{eff}\frac{\partial\phi}{\partial x_{j}}\Delta n_{j}\right)_{ip}+\overline{S_{\phi}}V \tag{23}$$

$$V\left(\frac{\rho u_{i}-\rho^{o}u_{i}^{o}}{\Delta t}\right)+\sum_{ip}\dot{m}_{ip}\left(u_{i}\right)_{ip}=\sum_{ip}\left(P\Delta n_{i}\right)_{ip}+\sum_{ip}\left(\mu_{eff}\left(\frac{\partial u_{i}}{\partial x_{j}}+\frac{\partial u_{j}}{\partial x_{i}}\right)\Delta n_{j}\right)_{ip}+\overline{S_{M_{i}}}V \tag{24}$$

$$V\left(\frac{\rho\phi-\rho^{o}\phi^{o}}{\Delta t}\right)+\sum_{ip}\dot{m}_{ip}\phi_{ip}=\sum_{ip}\left(\Gamma_{eff}\frac{\partial\phi}{\partial x_{j}}\Delta n_{j}\right)_{ip}+\overline{S_{\phi}}V \tag{25}$$

where V is the control volume, the subscript *ip* denotes an integration point, the summation is over all the integration points of the finite volume, Δnj is the discrete outward surface vector, Δt is the timestep. Note that the First Order Backward Euler scheme has been assumed in this equation, although a second order scheme is also available as discussed below. Superscripts *o* refers to the old time level. The discrete mass flow through a surface of the finite volume is denoted by $\dot{m}_{ip}$ and is given by (CFX, 2004):

$$\dot{m}_{ip}=\left(\rho U_{j}\Delta n_{j}\right)_{ip}^{o} \tag{26}$$

5.1 THE COUPLED SYSTEM OF EQUATION

The linear set of equations that arise by applying the Finite Volume Method to all elements in the domain are discrete conservation equations. The system of equations can be written in the form:

$$\sum_{nbi}a_{i}^{nb}\phi_{i}=b_{i} \tag{27}$$

where ϕ is the solution, *b* the right hand side, *a* the coefficients of the equation, *i* is the identifying number of the finite volume or node in question, and *nb* means " neighbor", but also includes the central coefficient multiplying the solution at the *i*th location. The node may have any number of such neighbors, so that the method is equally applicable to both structured and unstructured meshes. The set of these, for all finite volumes constitutes the whole linear equation system. For a scalar equation (e.g. enthalpy or turbulent kinetic energy), each a_i^{nb}, ϕ_{nb} and b_i is a single number. For the coupled, 3D mass-momentum equation set they are a (4 x 4) matrix or a (4 x 1) vector, which can be expressed as:

$$a_t^{nb} = \begin{bmatrix} a_{uu} & a_{uv} & a_{uw} & a_{up} \\ a_{vu} & a_{vv} & a_{vw} & a_{vp} \\ a_{wu} & a_{wv} & a_{ww} & a_{wp} \\ a_{pu} & a_{pv} & a_{pw} & a_{pp} \end{bmatrix}_t^{nb}, \quad \phi_t = \begin{bmatrix} u \\ v \\ w \\ p \end{bmatrix}_t \text{ and } \quad b_t = \begin{bmatrix} b_u \\ b_v \\ b_w \\ b_p \end{bmatrix}_t$$

It is at the equation level that the coupling in question is retained and at no point are any of the rows of the matrix treated any differently (e.g. different solution algorithms for momentum versus mass). The advantages of such a coupled treatment over a non-coupled or segregated approach are several: robustness, efficiency, generality and simplicity. These advantages all combine to make the coupled solver an extremely powerful feature of any CFD code. The principal drawback is the high storage needed for all the coefficients.

The program uses a Multigrid (MG) accelerated Incomplete Lower Upper (ILU) factorization technique for solving the discrete system of linearised equations. It is an iterative solver whereby the exact solution of the equations is approached during the course of several iterations.

The linearised system of discrete equations described above can be written in the general matrix form:

$$[A][\phi] = [b] \tag{28}$$

where [*A*] is the coefficient matrix, [□] the solution vector and [*b*] the right hand side.

The above equation can be solved iteratively by starting with an approximate solution, f^n, that is to be improved by a correction, □', to yield a better solution, f^{n+1}, i.e.

□$^{n+1}$ = □*n* + □'

where is a solution of with *rn*, the residual, obtained from, Repeated application of this algorithm will yield a solution of the desired accuracy. By themselves, iterative solvers such as ILU tend to decrease rapidly in performance as the number of computational mesh elements increases. Performance also tends to decrease rapidly if there are large element aspect ratios present. The performance of the solver can be greatly improved by employing a technique called 'multigrid' (CFX, 2004).

6 THE HYDRAULIC JUMP

The Hydraulic Jump is a phenomenon that is formed whenever flow changes from supercritical to sub critical flow. In this transition from supercritical to sub critical flow, water surface rises abruptly, surface rollers are formed, intense mixing occurs, air is entrained, and a large amount of energy is usually dissipated. By utilizing these characteristics, a hydraulic jump can be used to dissipate energy, to mix chemicals, or to act as an aeration device (CHAUDHRY, 1993).

The Figure 4 represents the hydraulic jump characteristics that occur in horizontal or in small-sloped channels for transient flow. There is reduction average velocity, in direction to the flow, with a presence of a turbulence accentuated. If the raise of water surface is high, the surfaces in the section of hydraulic jump make almost regular water eddies in relatively control volume position. The water mass buoyancy advances the air entrainment in the flow appear the air bubbles. The turbulence in hydraulic jump and the eddy movement produce important energy dissipation (PORTO, 2004).

The hydraulic jump is confined between the flow depths upstream, where the flow is torrential, and downstream, where the flow is fluvial, which the pressure distribution is hydrostatic. The flow depths upstream, y_1, and downstream, y_2, of the jump are called *sequent depths*, or *conjugate depths*. The difference, $y_2 - y_1$, is called *hydraulic jump depths* and it is an important parameter in hydraulic jump characterization like energy dissipater. The height difference in the energy line ΔE is called *hydraulic jump energy loss* (CHAUDHRY, 1993).

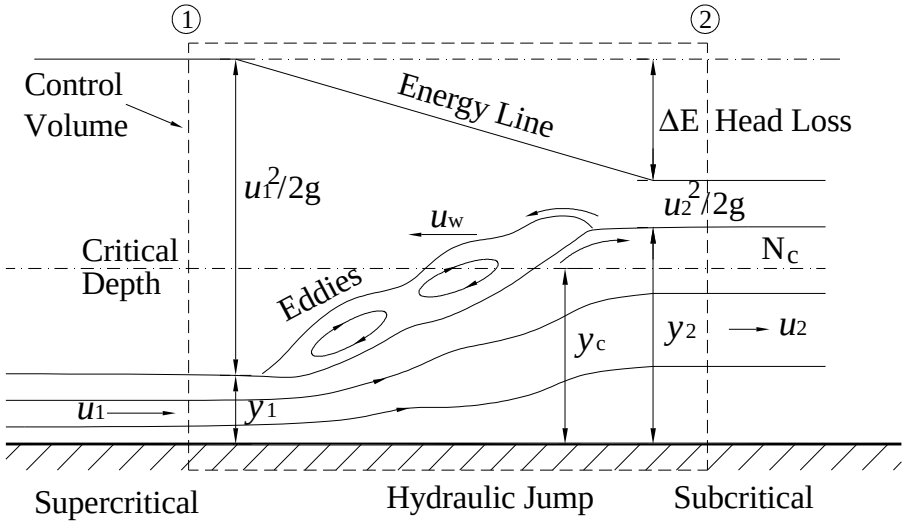

Figure 4. Hydraulic Jump (PORTO, 2004).

To simplify the derivation, consider a rectangular, horizontal channel will be considered, as our problem. Since the amount of energy loss in the jump is not known firstly, it cannot be applied the energy equation directly. In transient flow, the momentum theorem shows that all forces in control volume mobile are equal to the momentum flow on the control surface. Therefore, on control of mobile volume operates the pressure distribution forces in section 1 and 2 in according to Figure 4. This way, the one-dimensional flow can be expressed as (PORTO, 2004):

For relatively velocity (u_{rel}) on control of mobile volume:

Section 1: $u_{rel} = u_1 + u_w$

Section 2: $u_{rel} = u_2 + u_w$

Continuity: $\int_{CS} (\rho \boldsymbol{u}.dA) = 0 \rightarrow (u_1 + u_w)y_1 = (u_2 + u_w)y_2$ (29)

Momentum: $\sum F_x = \int_{SC} \boldsymbol{u}(\rho \boldsymbol{u} dA)$ or

$$F_1 - F_2 = -\rho(u_1 + u_w)A_1(u_1 + u_w) + \rho(u_2 + u_w)A_2(u_2 + u_w) \quad (30)$$

where: $A_1 = b.y_1$ and $A_2 = b.y_1$ are section area in 1 and 2; b is width of rectangular channel.

Of the Static of Fluids, the force on a plain region is given by: $F = \rho.g.\bar{y}.A$, on which, $\bar{y} = \frac{y}{2}$ is the vertical distance between the free surface and the gravity center in the section, therefore:

$$g.\bar{y}_1 A_1 - g.\bar{y}_2 A_2 = -(u_1 + u_w)A_1(u_1 + u_w) + (u_2 + u_w)A_2(u_2 + u_w) \quad (31)$$

For rectangular section the equation 31 can be written as:

$$\frac{1}{2}g.(y_1^2 - y_2^2) = -(u_1 + u_w)^2 y_1 + (u_2 + u_w)^2 y_2 \quad (32)$$

Using the continuity:

$$\frac{1}{2}(y_1^2 - y_2^2) = -\frac{1}{g}(u_1 + u_w)^2 y_1 + \frac{1}{g}(u_1 + u_w)^2 \frac{y_1^2}{y_2^2} y_2 \quad (33)$$

or

$$c = u_1 + u_w = \sqrt{\frac{g.y_2}{2.y_1}(y_1 + y_2)} \quad (34)$$

where: c is celerity.

In equation 34, if $u_w = 0 \rightarrow \frac{u_1}{\sqrt{g.y_1}} = \sqrt{\frac{y_2}{2.y_1}\left(1 + \frac{y_2}{y_1}\right)}$ (35)

Now, the Froude number, $Fr_1 = \frac{u_1}{\sqrt{gy_1}}$, Hence, Eq 35 may be written as:

$$\left(\frac{y_2}{y_1}\right)^2 + \frac{y_2}{y_1} - 2Fr_1^2 = 0 \quad (36)$$

Solution of this equation yields [6].

$$\frac{y_2}{y_1} = \frac{1}{2}\left(-1 + \sqrt{1 + 8Fr_1^2}\right) \quad (37)$$

Note that the negative sign with the radical term is neglected because it given a negative ratio, which is physically impossible. This equation specifies a relationship between the depths upstream of the jump in terms of Fr_1. Proceeding similarly; we can derive the following equation in terms of Fr_2 (CHAUDHRY, 1993).

$$\frac{y_1}{y_2} = \frac{1}{2}\left(-1 + \sqrt{1 + 8Fr_2^2}\right) \quad (38)$$

7 NUMERICAL SIMULATION

The purpose of this paper is two-fold. First, it is intended to demonstrate that certain known complex features of the hydraulic jump can be resolved. Secondly, it is intended to compare numerical results with experimental data. To solve the problem it has been used the Reynolds Stress Model for multiphase Free Surface.

As it is shown in Figure 4, the geometry of the problem is:

- y_1 = 0,0372 m; y_2 = 0,1800 m; b = 0,1000 m and l (length) = 3,0000 m.

110 The simulation could be divided in two parts: First of all, for wave formation to introduce a velocity smaller than that velocity for Froude number for steady hydraulic jump; second, it has been used the velocity for steady wave in hydraulic jump after 3 seconds of simulation. This Froude Number (Fr_1 = 3,76) defines a transitory hydraulic jump, which characterizes an oscillatory upstream in the surface of hydraulic jump.

The mesh used for simulation is presented in Figure 5. On the left, it is shown the entire domain and on the right there is the vertical detail of mesh. On the button it has been used mesh cell of 0,01 m and on the top the mesh cell is about 0,05 m.

The domain, Fluids and Simulation characteristics as well as the initial and boundary conditions are shown in Table 1.

Table 1: The Domain, Fluids and Simulation characteristics, initial and boundary conditions.

	Domain			
	Number of Nodes		65 362	
	Number of Tetrahedrons Elements		354 004	
	Number of Faces		16 616	
	Fluids			
	Water		Air	
	Temperature	25 ^oC	Temperature	25 ^oC
	Dynamic Viscosity	8,899*10^{-4} kg.m^{-1}.s^{-1}	Dynamic Viscosity	1,831*10^{-5} kg.m^{-1}.s^{-1}
	Density	998 kg.m^{-3}	Density	1,185 kg.m^{-3}
	Surface Tension Coef.	0,0732 N.m^{-1}		
	Simulation			
	Time step		0,005 s	
	Simulation Time		6,6 s	
	Process Characteristic		Two Processor In Parallel	
	CPU Time Processing		4,61*10^6 s	
	Boundary and Initial Conditions			
Button and sides	Walls			
	Top	Opening		
Inlet (t < 3 s)	u(Water) = 1,0 m.s^{-1}; u(Air) = 0; v(Water) = 0; v(Air) = 0; w(Water) = 0; w(Air) = 0; p(Water) = ρ.g.y_1 – ρ.g.y; p(Air) = 0			
Inlet (t > 3 s)	u(Water) = 2,27 m.s^{-1}; u(Air) = 0; v(Water) = 0; v(Air) = 0; w(Water) = 0; w(Air) = 0; p(Water) = ρ.g.y_1 – ρ.g.y; p(Air) = 0			
Outlet	du/dx(Water) = 0; du/dx(Air) = 0; dv/dx(Water) = 0; dv/dx(Air) = 0; dw/dx(Water) = 0; dw/dx(Air) = 0; p(Water) = ρ.g.y_2 – ρ.g.y; p(Air) = 0			
Initial Condition	u(Water) = 1,0 m.s^{-1}; u(Air) = 0; v(Water) = 0; v(Air) = 0; w(Water) = 0; w(Air) = 0; p(Water) = ρ.g.y_1 – ρ.g.y; p(Air) = 0			

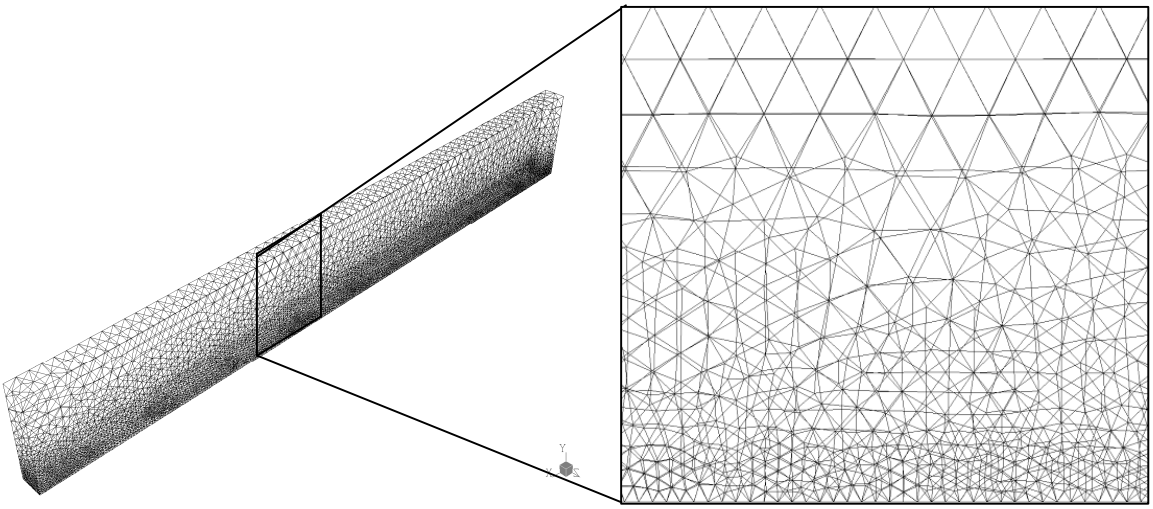

Figure 5. Mesh used in Numerical Simulation.

8 RESULTS

The numerical results obtained are showed in fig.6 to 8, after 6 seconds of simulation. In fig.6 the fraction of water volume in relation to the air volume, or it is, the value 1.00 represents the presence of 100% of water and 0.00 represents 0% of water or 100% of air.

Fig. 7 shows the formed pressure on field. The profile of hydraulic jump downstream joins closely with the static pressure or is slightly bigger. The oscillatory wave formed by the hydraulic jump regime provokes this increase of pressure.

Figure 8 presents the velocity field in every channel domain in a lateral view. In the entrance region the highest flow velocity can be observed in the channel and the formation of velocity profiles development. The formation of oscillations on the upstream amount on the free hydraulic jump is due to the instabilities caused by the superficial tension (instability of Kelvin-Helmholtz) and more predominantly the gravitational effect (instability of Rayleigh-Taylor) (LESIEUR, 1996).

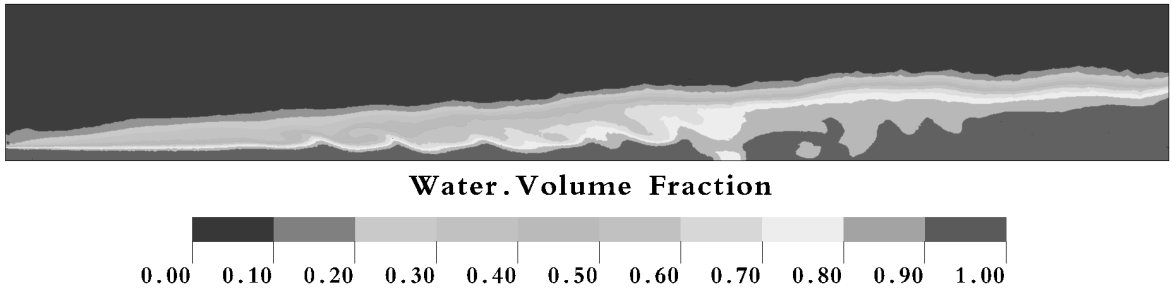

Figure 6. Volume Fraction of Water in Hydraulic Jump.

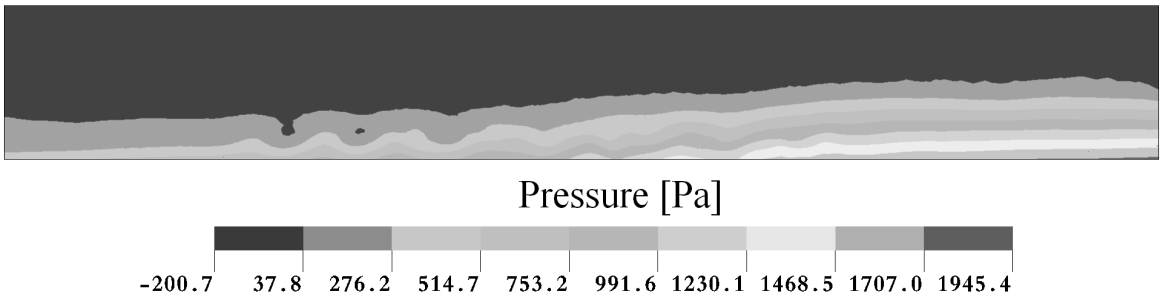

Figure 7. Pressure in Hydraulic Jump.

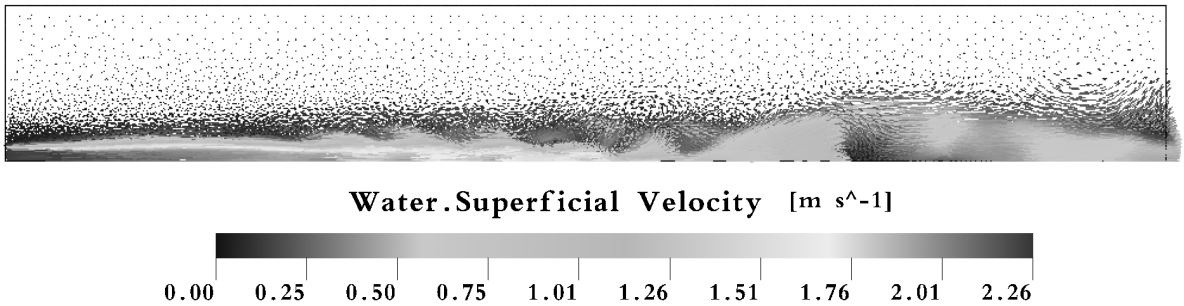

Figure 8. Velocity in Hydraulic Jump.

The wave propagation of hydraulic jump generation is shown in fig. 9 in a break of 0.5 to 3.0 seconds. As it can be observed in frames of free surface for 90% of water a wave dislocates from downstream to the amount upstream. It happens because of the high inflow and outflow fixed physically as well as because of the entrance velocity that establish the number of Froude, which provide the formation of so called positive wave of downstream.

The simulation was interrupted after wave formation (3 sec.), when the velocity of inflow has been increased for steady hydraulic jump generation – Figure 10. A new wave has been introduced, a negative upstream wave, which crash against earliest wave (negative downstream wave) – frame of t = 4.0 sec. In the next frame (for t = 5.0 sec), the only one wave was formed and, finally, the quasi-steady wave generated is shown in the final frame (for t = 6.0 sec) – Figure 10.

Oscillatory waves on the upstream of hydraulic jump as showed in Figure 11(a), which represents a gravitational wave like the oceanic giants waves (tsunamis) (INGARD, 1988) (PENNA, 1984). The obtained Froude Number (Fr_1 = 3.76) define a transitory hydraulic jump which characterize an oscillatory upstream on the surface of hydraulic jump, is shown in Figure 11(b). The turbulence behavior of the free surface is also visualized in figure 11(b), which is responsible for the air carried in to the flow.

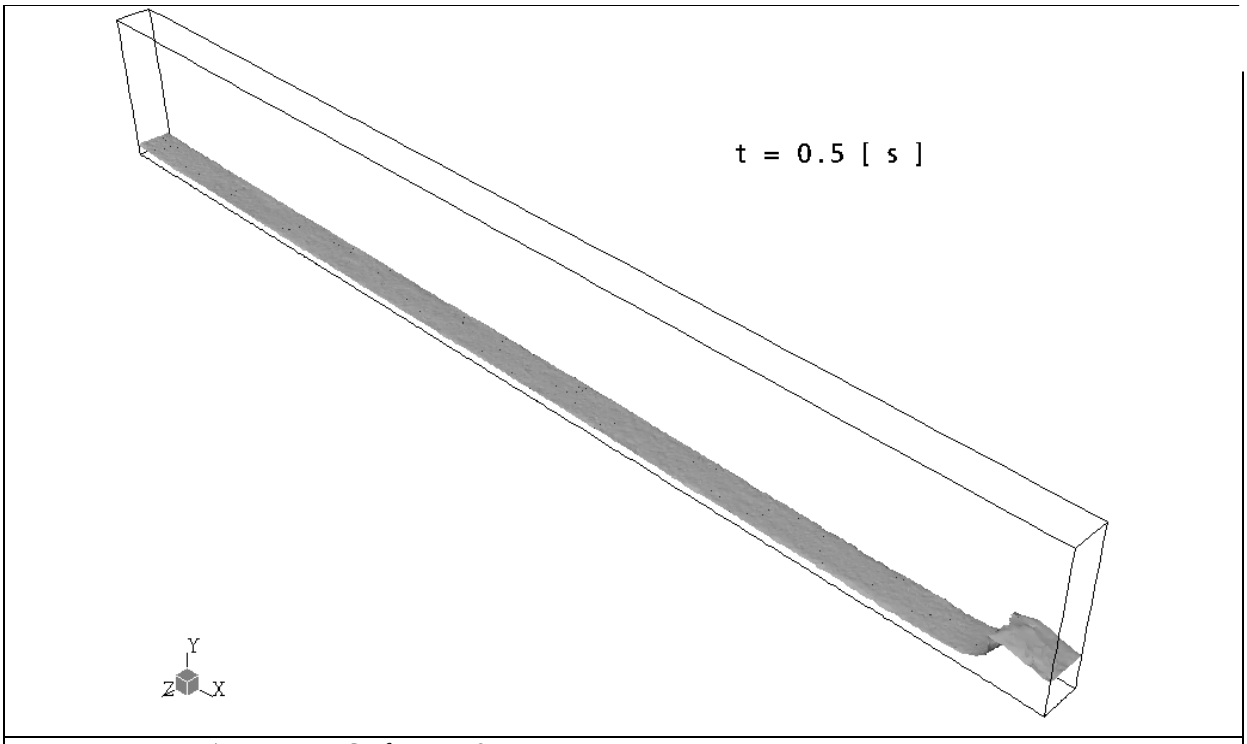

a) Free Surface: t = 0,5sec.

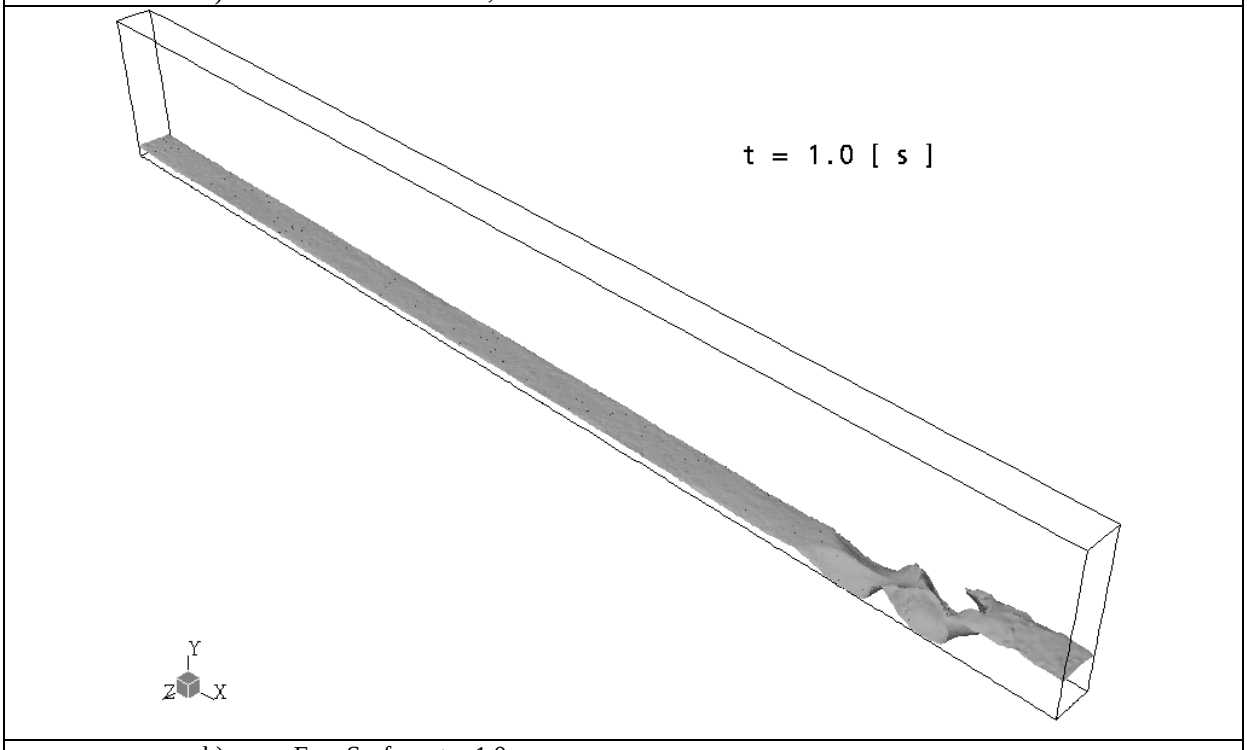

b) Free Surface: t = 1,0sec.

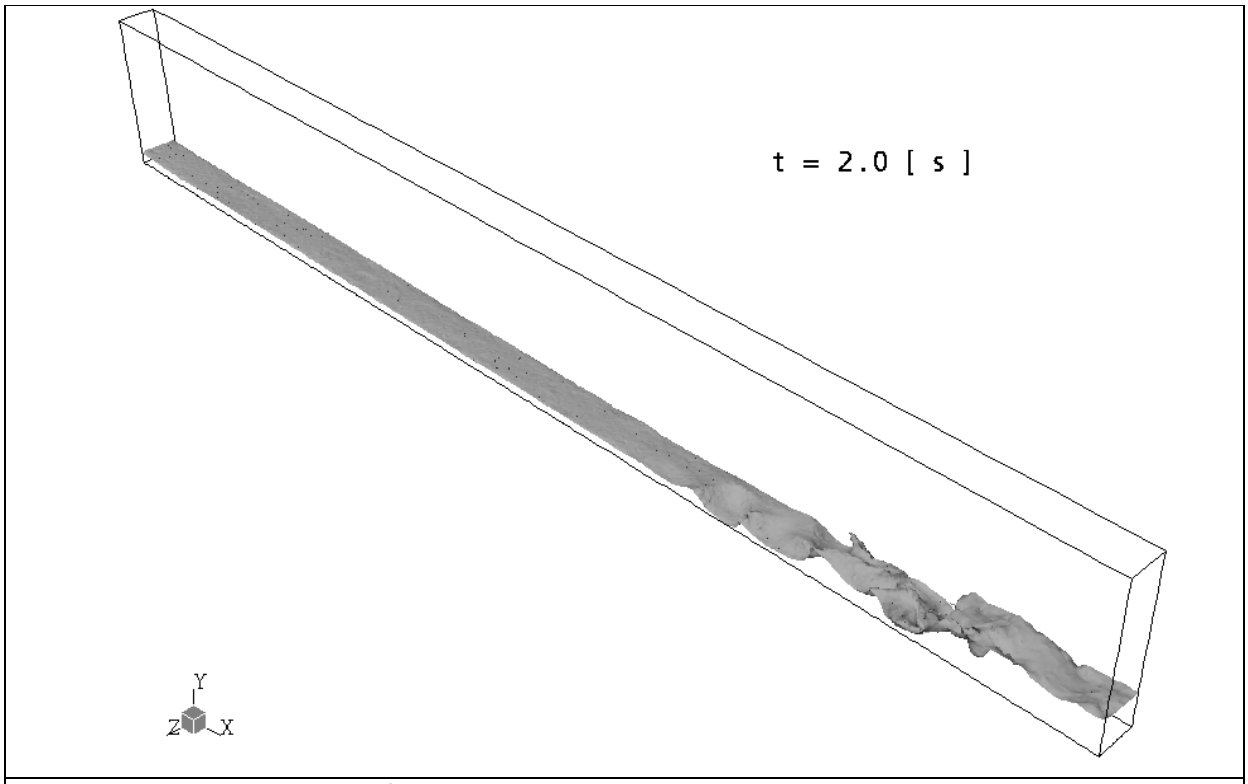

c) Free Surface: t = 2,0sec.

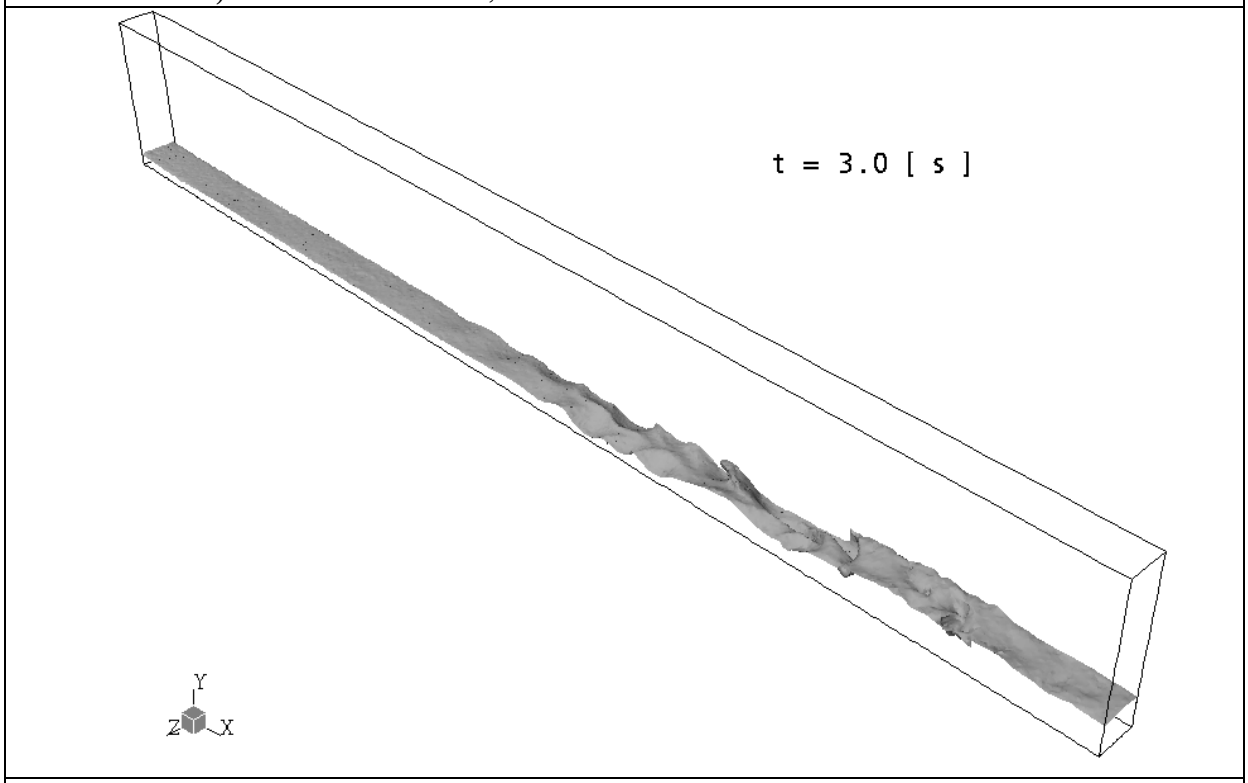

d) Free Surface: t = 3,0sec.

Figure 9: Free Surface in Hydraulic Jump Generation: a) t=0,5sec; b) t=1,0 sec; c) t=2,0sec and d) t=3sec.

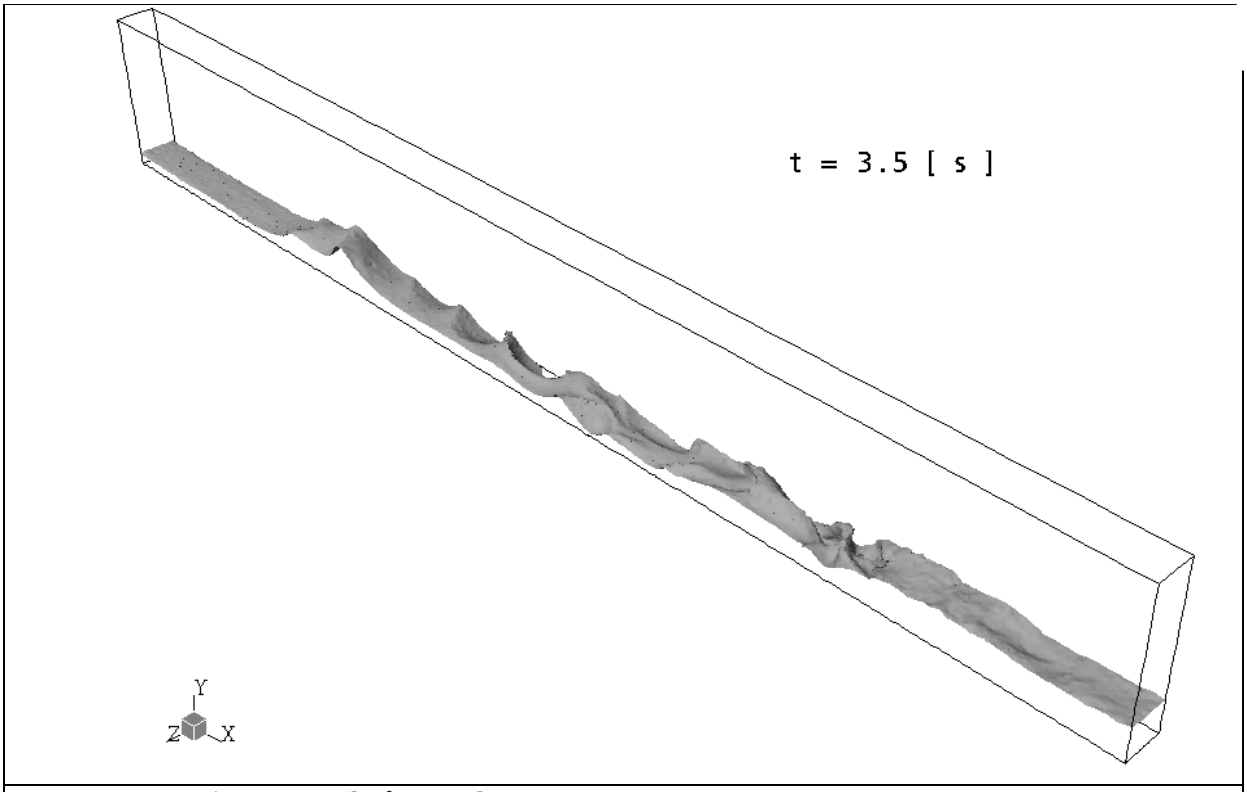

a) Free Surface: t = 3,5sec.

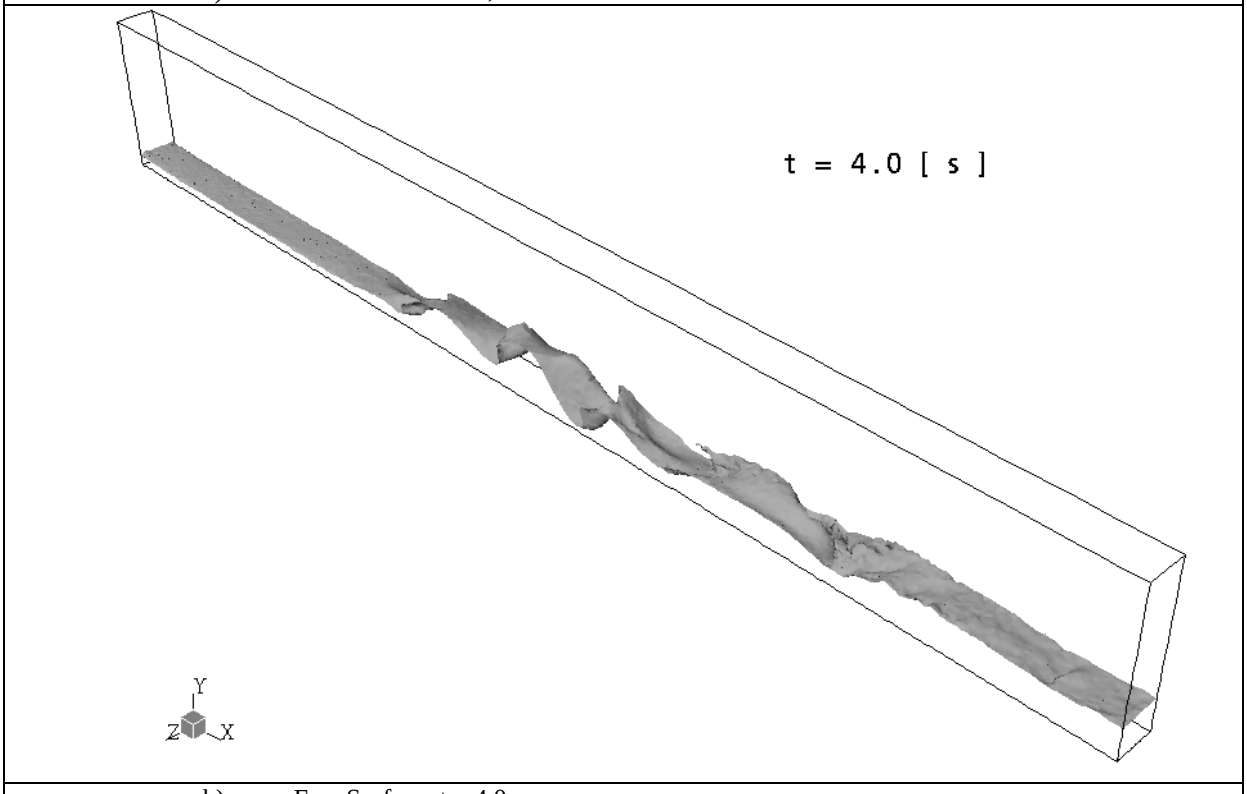

b) Free Surface: t = 4,0sec.

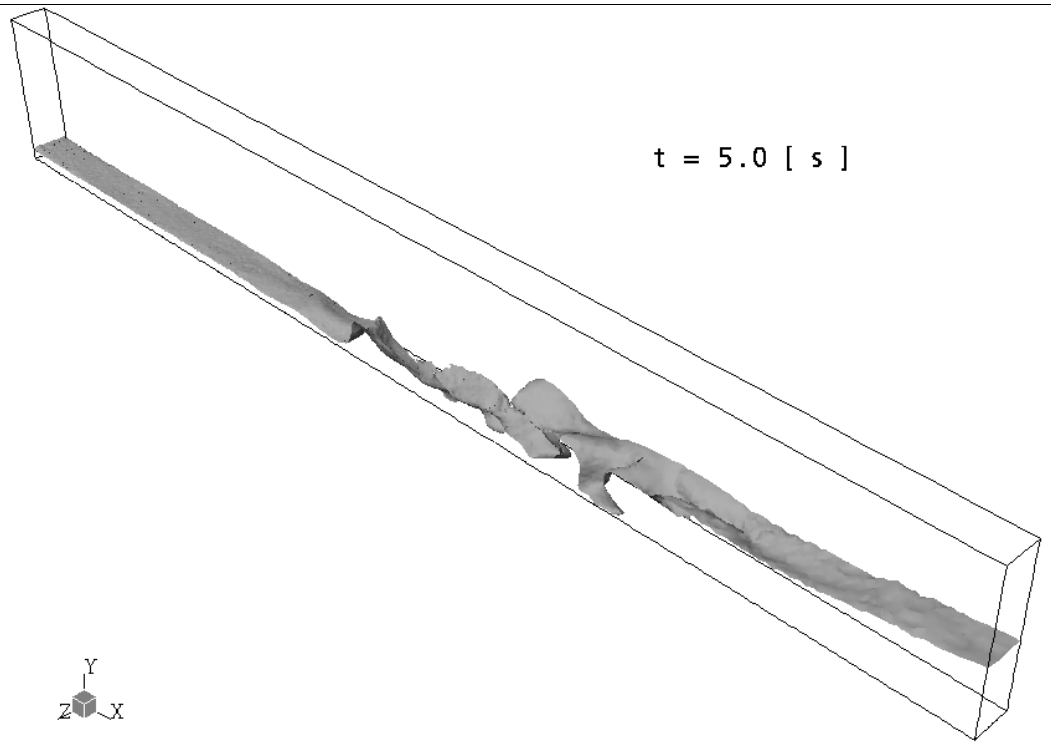

c) Free Surface: t = 5,0sec.

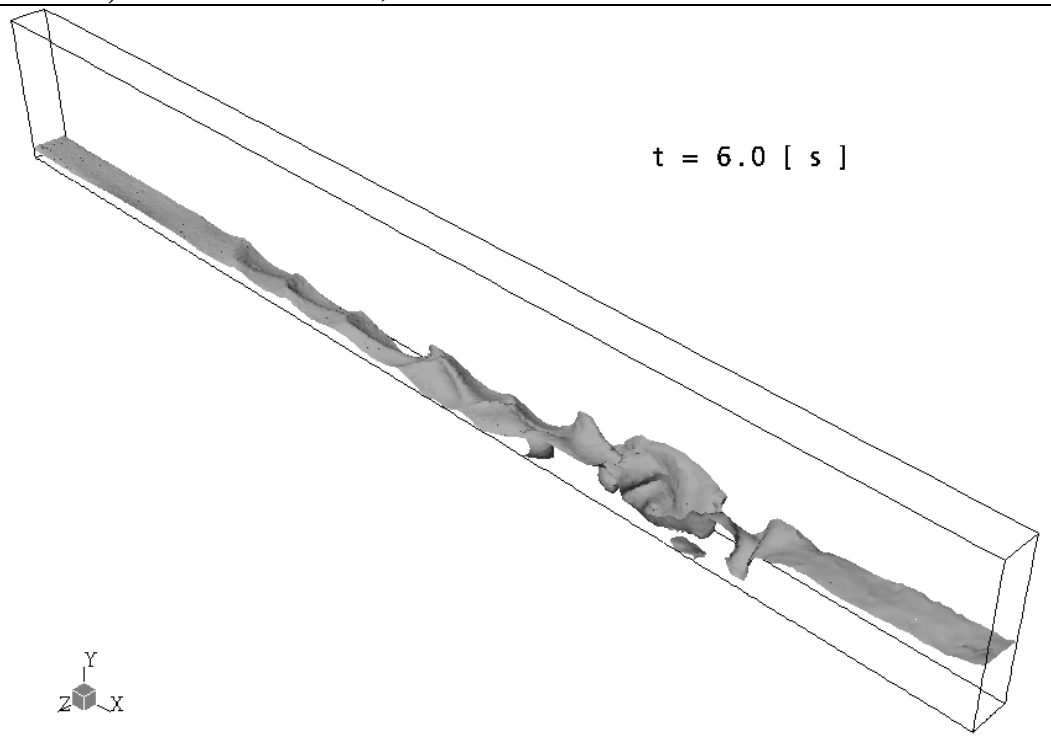

d) Free Surface: t = 6,0sec.

Figure 10: Free Surface in Transitional Hydraulic Jump Generation: a) t = 3,5sec; b) t = 4,0 sec; c) t = 5,0sec and d) t = 6sec.

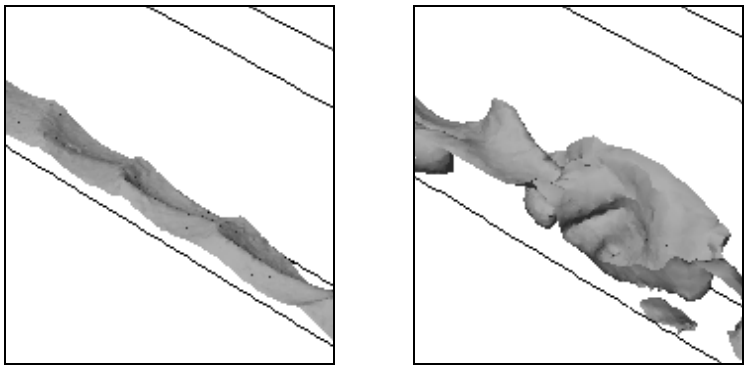

(a) (b)

Figure 11. Gravitational Instability (a) and Turbulence Effect in Free Surface (b).

The Figure 12, shows the agreement between experimental data and numerical results. As it is shown, the free surface in the experimental data presents two different behaviors: in upstream, the level of agreement is higher than in the hydraulic jump. Therefore, in the first experimental data line was immerged in to 90% of volume fraction of water region. By the other hand, on the hydraulic jump, the experimental free surface is in between 70 e 80% volume fraction of water region.

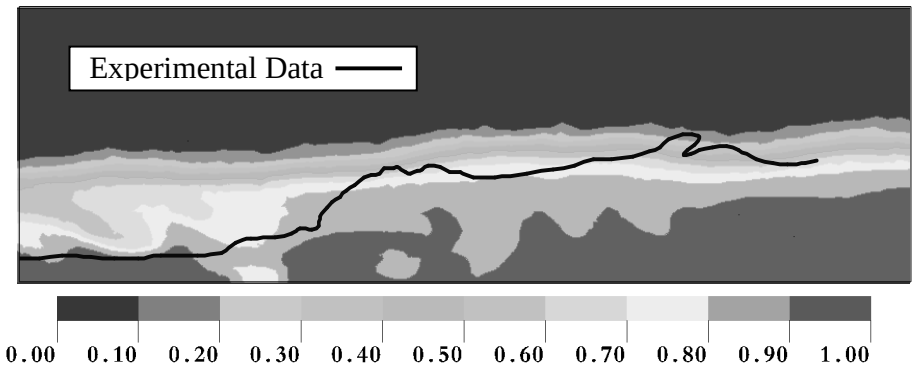

Figure 12. Experimental [3] and Numerical Data Comparison.

9 CONCLUSIONS

Computational Fluid Dynamics (CFD) is a computer-based tool for simulating the systems behavior involving fluid flow. A CFD program has been used to simulate a hydraulic problem. A numerical simulation was performed to a hydraulic jump with a determinate geometry and this simulation has demonstrated that certain known complex features of hydraulic jump can be resolved. In the results of simulation was presented the hydraulic characteristics as: pressure field, velocity field and the water volume fraction of the channel. The frames of the transient simulation were presented and the waves formed in the procedure of simulation was denoted and explained. Firstly, a positive downstream wave is formed for hydraulic jump generation. This simulation was interrupted after wave formation (3 sec.), when the velocity of

inflow was increased for steady hydraulic jump generation. A new wave was introduce, a negative upstream wave, which crashed against earliest wave (negative downstream wave). Gravitational waves were visualized in the upstream of the hydraulic jump; these oscillatory waves in the upstream of hydraulic jump represent a gravitational wave like the oceanic giant waves (tsunamis). The turbulence behavior of the free surface is also visualized, this phenomena is responsible for the air carried in to the flow. A comparison of the numerical results with experimental data was showed for validation of the simulation. Two different behaviors are showed in this comparison: the free surface in the experimental data presents the level of upstream agreement higher than in the hydraulic jump. Therefore, in the first the experimental data line was immerged in to 90% of volume fraction of water region. By the other hand, in the hydraulic jump, the experimental free surface is in between 70 e 80% volume fraction of water region. As conclusion of this problem in hydraulic engineering, it can be said that the Computational Fluid Dynamic represents a good approximation for this hydraulic jump phenomenon.

ACKNOWLEDGEMENTS

The authors would like to thanks to Engineering Simulation and Scientific Software (ESSS), by means of Formula Team SAE from Sao Carlos Engineering School, which ceded CFX license.

REFERENCES

CFX (2004). *CFX 5 Solver Theory*. Ansys Canada Ltda, Waterloo, Ontario, Canada. 250 p.

LESIEUR, MARCEL. (1996). Turbulence in Fluids. Kluwer Academic Publishers.

WILCOX, D.C.(2000), Turbulence Modeling for CFD. DCW Industries, 2000, p. 314.

LAUNDER, B.E., REECE, G.J. AND RODI, W. (1975). Progress in the developments of a Reynolds-stress turbulence closure. J. Fluid Mechanics, Vol. 68, pp.537-566.

SMAGORINSKY, M. J. (1963) General Circulation Experiments with the Primitive Equations. I. The Basic Experiment. *Month. Wea. Rev.*, 91:99-164.

CHAUDHRY, M. H. (1993). Open Channel Flow. Prentice Hall, New Jersey, 481 p.

PORTO, R. M. (2004). Hidráulica Básica. Projeto REENGE. 519 p. (in Portuguese).

INGARD, K. U. (1988). Fundamentals of Waves and Oscillations. Cambridge University Press.

PENNA, J. A. (1984). Study on the hydraulic fast mixture influence in the flocculation of the supply water. Masters degree dissertation in University of São Paulo. Brazil. 150 p (in Portuguese).